Ion-molecule reaction dynamics: Velocity map imaging studies of N^+ and O^+ with CD_3OD

Linsen Pei and James M. Farrar[a)]
Department of Chemistry, University of Rochester, Rochester, New York 14627, USA

(Received 27 April 2015; accepted 10 August 2015; published online 25 August 2015)

We present a study of the charge transfer reactions of the atomic ions N^+ and O^+ with methanol in the collision energy range from ~2 to 4 eV. Charge transfer is driven primarily by energy resonance, although the widths of the product kinetic energy distributions suggest that significant interchange between relative translation and product vibration occurs. Charge transfer with CD_3OD is more exoergic for N^+, and the nascent parent ion products appear to be formed in excited $\tilde{B}$ and $\tilde{C}$ electronic states, and fragment to CD_2OD^+ by internal conversion and vibrational relaxation to the ground electronic state. The internal excitation imparted to the parent ion is sufficient to result in loss of one or two D atoms from the carbon atom. The less exoergic charge transfer reaction of O^+ forms nascent parent ions in the excited $\tilde{A}$ state, and internal conversion to the ground state only results in ejection of single D atom. Selected isotopomers of methanol were employed to identify reaction products, demonstrating that deuterium atom loss from nascent parent ions occurs by C–D bond cleavage. Comparison of the kinetic energy distributions for charge transfer to form CD_3OD^+ and CD_2OD^+ by D atom loss with the known dynamics for hydride abstraction from a carbon atom provides strong evidence that the D loss products are formed by dissociative charge transfer rather than hydride (deuteride) transfer. Isotopic labeling also demonstrates that chemical reaction in the $N^+ + CD_3OD$ system to form $NO^+ + CD_4$ does not occur in the energy range of these experiments, contrary to earlier speculation in the literature. © *2015 AIP Publishing LLC.* [http://dx.doi.org/10.1063/1.4929389]

I. INTRODUCTION

The cations N^+ and O^+ are the primary atomic ions in the Earth's ionosphere, and with recombination energies of 14.53 and 13.62 eV, respectively, exhibit high reactivity with a wide range of molecular collision partners. The charge transfer and particle transfer reactions of these species with the primary constituents of the atmosphere have been the subject of numerous investigations.[1–4] The reactions of O^+ with small hydrocarbons have been examined as potential models for spacecraft surface degradation in low earth orbit (LEO).[5] Early studies of the reaction rates of N^+ and O^+ with several small molecules found in the troposphere and the stratosphere have reported rate constants near the Langevin limit.[6,7] Because molecular species present at lower altitudes may diffuse to the ionosphere and undergo subsequent reactions with N^+ and O^+, there is interest in and justification for measuring reaction rates of these ions with the large number of molecules that are implicated in atmospheric chemistry. Moreover, in such chemically complex environments, the products of one reaction often serve as reactants in a subsequent process. Because bimolecular reaction rates may have a significant dependence on the internal energy distributions of reactants,[8] experiments that probe energy disposal and the dynamics of ion-molecule interactions provide an important complement to rate constant measurements of atmospherically significant reactions.

The orbital occupancies and spin states of the N^+ and O^+ ions play an important role in determining their reactivities, particularly atom transfer and bond formation reactions. Hund's rule dictates that the ground state electron configurations of N^+ and O^+ are high spin, ^3P and ^4S, respectively, but excited states of lower multiplicity may interact with ground state surfaces to generate chemistry determined by motion on coupled potential energy surfaces. A recent study from our group[9] on the $O^+ + CH_3X$ system (X = Cl, Br, I) showed that spin-changing transitions from quartet to doublet states are facilitated by heavier halogen atoms and allow halide transfer to O^+ to occur. A number of rate measurements of N^+ and O^+ with organic molecules[6,7] have shown that charge transfer is a particularly important channel, but there has been some ambiguity about reactive pathways for producing fragment ions. Several studies of N^+ and O^+ reactions with hydrogen-containing molecules, denoted RH,[5,7,10–15] have suggested that hydride abstraction to form NH or OH + R^+ in an exoergic process is the preferred pathway for R^+ formation, rather than dissociative charge transfer. Although the formation of the N–H or O–H bond makes these channels thermodynamically favorable, only the ground state N^+ system has a vacant orbital to accommodate the electron pair donated by the hydride ion. Previous work from other laboratories and from ours[16–19] has demonstrated that the dynamics of hydride transfer are significantly different from dissociative charge transfer that measurements of energy disposal may allow a distinction between the processes. The ubiquity of hydride abstraction in these systems has remained an open question.

a)Author to whom correspondence should be addressed. Electronic mail: farrar@chem.rochester.edu.

Specifically, studies of thermal rates of N^+ and O^+ with CH_3OH[7,20] have yielded large rate constants in excess of 10^{-9} cm^3 s^{-1} molecule^{-1}, but have raised several important questions. The observations of product ions corresponding to loss of a hydrogen atom from the parent CH_3OH^+ have been interpreted inconsistently in earlier publications. In some papers, the reactions of N^+ or O^+ with CH_3OH to form CH_3O^+ or CH_2OH^+ are ascribed to hydride transfer. The possibility of forming these ions by dissociative charge transfer, where the nascent ionic CH_3OH^+ product ejects a hydrogen atom, appears to be overlooked, largely because hydride transfer is more exoergic. Second, although loss of hydrogen from CH_3OH^+ by C–H bond cleavage is less endoergic than loss of hydrogen by O–H bond scission, some papers are unclear about whether the reaction product is the hydroxymethyl cation, CH_2OH^+, or the higher energy methoxy cation, CH_3O^+. Finally, the reaction of N^+ with CH_3OH has been reported to form NO^+.[6] However, this conclusion is not supported by direct observation of NO^+, but through the biexponential time dependence of the rate of appearance of m/e = 30 products.

In this paper, we present a crossed beam study of the products of the primary charge transfer reactions and secondary fragmentation processes occurring in collisions of N^+ and O^+ with CD_3OD and selected isotopomers. With appropriate choice of isotopomers, we show that we can distinguish between removal of a hydrogen atom from carbon or oxygen. The velocity map imaging method of product detection[21] yields energy and angular distributions for reaction products, allowing us to determine the nature of the initial electron transfer process and the isomeric identities of the products of the fragmentation/abstraction process. In addition, we present direct evidence that NO^+ formation does not occur in the N^+ + methanol system, in contradiction to earlier reports in the literature.

The specific reactions we have studied, along with reaction thermochemistry, are summarized here[22]

$$N^+(^3P) + CD_3OD \rightarrow N + CD_3OD^+ \Delta H = -3.69 \text{ eV}, \quad (1)$$
$$\rightarrow N + D + CD_2OD^+ \Delta H = -2.70, \quad (2)$$
$$\rightarrow N + D_2 + CDOD^+ \Delta H = -2.20, \quad (3)$$
$$O^+(^4S) + CD_3OD \rightarrow O + CD_3OD^+ \Delta H = -2.78, \quad (4)$$
$$\rightarrow O + D + CD_2OD^+ \Delta H = -1.78. \quad (5)$$

II. EXPERIMENTAL

The experiment is performed with a crossed beam instrument equipped with a velocity map imaging (VMI) detector,[21] described in previous work from our laboratory.[23] The imaging system measures all product velocities in the plane of the beams for a given mass in a single detection time interval. Product ions are detected mass-selectively by varying the delay time between extraction and detection. The experimental method is similar to schemes employed in other laboratories.[24–29]

A continuous ion beam of N^+ or O^+ cations is prepared by electron impact[30] on a mixture of ~10% N_2 or CO in He. The primary product of electron impact on this mixture is He^+, which then undergoes charge transfer with N_2 or CO to form both parent and fragment cations. The N^+ or O^+ cations thus formed have been determined to be in their ground electronic states.[31,32] These atomic ions are extracted, mass selected, and decelerated and focused by a series of ion optics, and delivered to the volume defined by the repeller and extraction electrodes of a velocity map imaging detector. The ion beam has a roughly triangular kinetic energy distribution with a FWHM of approximately 0.2 eV for O^+ and 0.5 eV for N^+ in the laboratory frame of reference. The neutral beam is produced by a pulsed solenoid valve located 10 mm upstream from a 1 mm skimmer that expands a mixture of CD_3OD or CH_3OD (Cambridge Isotope Laboratories) seeded in He carrier gas at 1 atm pressure. The pressure in the collision chamber is $\sim 2 \times 10^{-7}$ Torr with the beams running.

The reactant beams intersect at the center of a collision volume of dimensions (3 mm)^3 bounded by two circular electrodes of radius 38 mm spaced by 20 mm. The lower, repeller electrode and the upper, extractor electrode are maintained at ground potential as the ion and neutral beams intersect. The imaging detection scheme[21] employs the two-electrode geometry described by Suits *et al.*[33] Delayed pulsed extraction is achieved with high voltage pulses applied to the repeller and the extractor with separate pulse generators (DEI PVX-4140, 4150) that are synchronized to the arrival of the central portion of the pulsed molecular beam. The pulses have rise times and durations of 25 ns and 1 to 2 μs, respectively, to allow all products to leave the volume between the repeller and extractor during the pulses.

The voltage on the repeller plate, V_1, is typically pulsed to +2300 V, the precise value dependent on transverse velocity and the filling factor for the MCP detector. The voltage V_2 on the extraction electrode is pulsed to a value $V_2 = 0.65\ V_1$. This electrode has a 13 mm aperture. A grounded electrode with a 20 mm aperture placed 13 mm above the extraction electrode provides velocity mapping for the product ions at the imaging plane, located 0.6 m downstream from the grounded lens.

Prior to striking the imaging plane of the detector, defined by the front face of a pair of chevron-mounted microchannel plates, the ions pass through a grounded grid. The MCPs are gated by a pulse of variable width, chosen to allow the full three-dimensional ion cloud associated with products of a single mass to be collected on the two-dimensional surface of the MCP anode. This signal is encoded as a light image by the phosphor screen following the MCP anode, and is recorded by a CCD camera (uEye 2230). The image is sent via a USB interface to a lab computer controlled by LabView software. A typical image represents the accumulation of 200 000 to 400 000 repetitions of the pulsed valve.

The finite thickness of the collision volume makes the largest experimental contribution to velocity resolution, a factor significantly more important than beam velocity distributions. Reaction products formed at various depths within the collision volume are accelerated to different extents and therefore do not satisfy a unique velocity-mapping condition.

III. RESULTS AND DISCUSSION

A. Parent ion formation

Velocity map images for collisions of N^+ and O^+ with CD_3OD were obtained at two collision energies, the first near

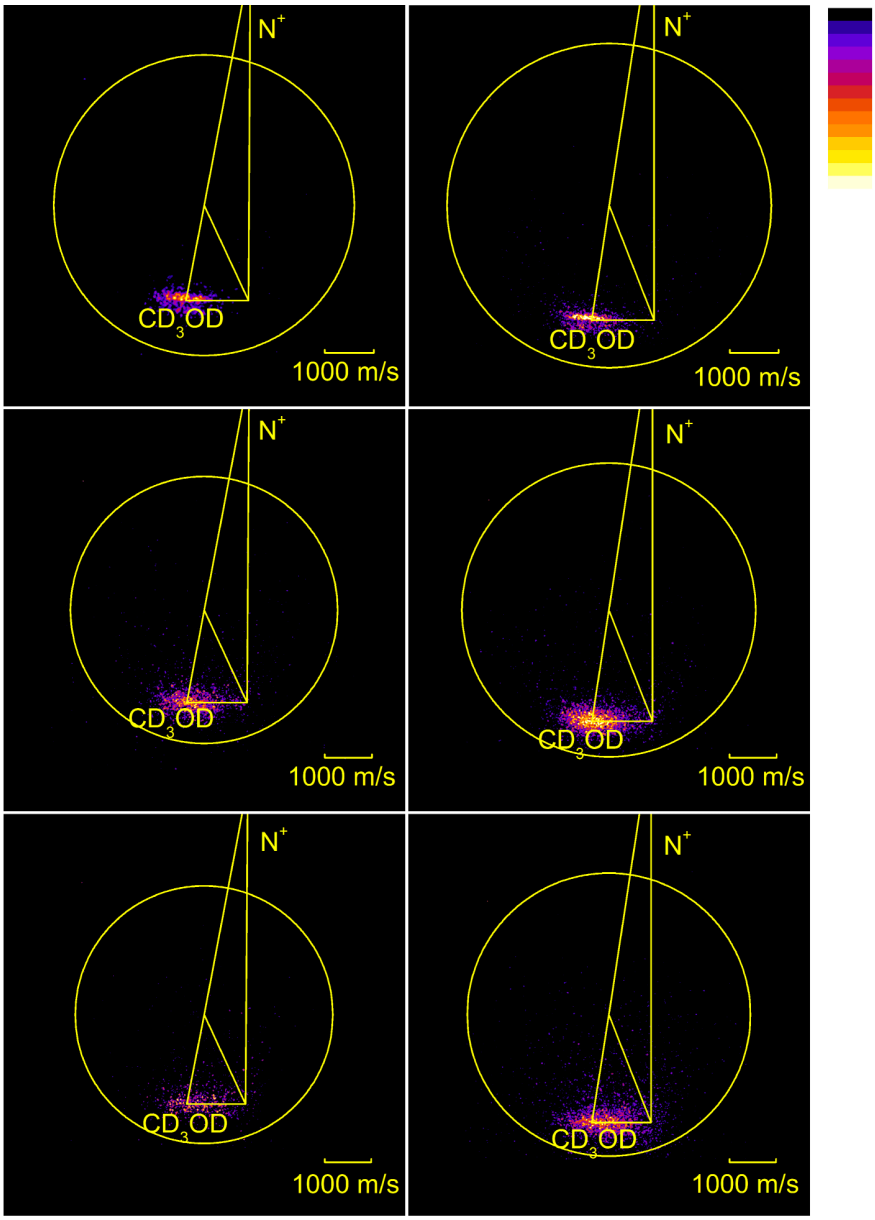

FIG. 1. Ion images for charge transfer and D-atom loss in the $N^+ + CD_3OD$ system, superimposed on the most probable Newton diagrams at a given collision energy. The left column of images corresponds to the formation of CD_3OD^+, CD_2OD^+, and $CDOD^+$ by charge transfer at a collision energy of 2.6 eV. The right column of images corresponds to the formation of those same products at a collision energy of 3.8 eV.

2 eV and the second near 4 eV. Figure 1 shows the velocity space images for the reactions of N^+ with CD_3OD superimposed on the kinematic Newton diagrams that define the laboratory velocities of the ion and neutral beams. The left column of images shows, from top to bottom, the formation of parent ions, ions formed by loss of a single D atom, and ions formed by loss of two D atoms, at a collision energy of 2.6 eV. A similar set of images at a collision energy of 3.8 eV is shown in the right column of the figure. The images show clearly that the parent ions resulting from charge transfer are formed in the immediate vicinity of the velocity of the neutral reagent, consistent with the behavior associated with resonant charge transfer, in which electron transfer takes place at long range on a time scale short in comparison with nuclear motion. The kinetic energies of reactants and products are essentially unchanged in such a collision.

Figure 2 shows a corresponding set of images for collisions of O^+ with CD_3OD. The left column of Figure 2, from top to bottom, shows images for primary charge transfer and D-atom loss at a collision energy of 2 eV. The right column shows images for those same processes at a collision energy of 3.8 eV. The image for loss of two D atoms is not intense enough for analysis. Similar to images from reactions with N^+, the images for the O^+ reactions show the same resonant charge transfer signature, although the velocity space images appear to be broader than their N^+ counterparts, reflecting significantly broader kinetic energy distributions as discussed below.

The images of Figures 1 and 2 encode reaction product angular and velocity distributions, which may be extracted from the data by first performing an inverse Abel transformation on the raw images.[34] Integration of the resulting product flux distributions $P(v_x, v_y)$ or $P(u_x, u_y)$, in lab coordinates or center of mass coordinates, respectively, over scattering angles yields product kinetic energy distributions via Eq. (6),

$$\langle P(E_T')\rangle_\theta = \int_0^\infty d\theta \sin\theta\, u\, P(u_x, u_y). \tag{6}$$

The relative kinetic energy distributions of the products of charge transfer are obtained easily, since momentum conserva-

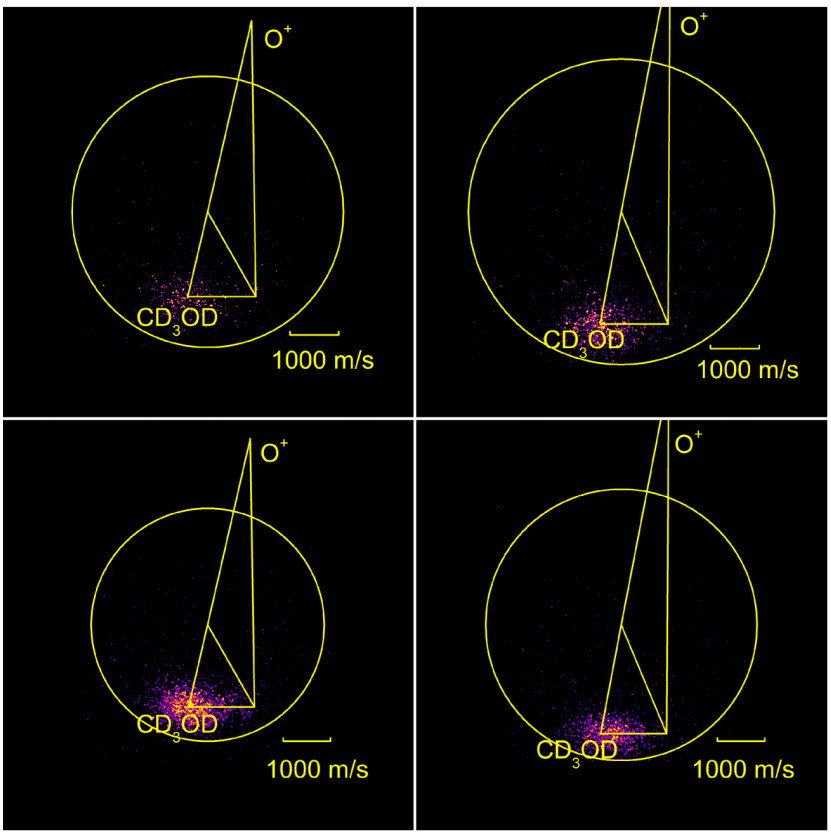

FIG. 2. Ion images for charge transfer and D-atom loss in the $O^+ + CD_3OD$ system, superimposed on the most probable Newton diagrams at a given collision energy. The left column of images corresponds to the formation of CD_3OD^+ and CD_2OD^+ by charge transfer at a collision energy of 2.0 eV. The right column of images corresponds to the formation of those same products at a collision energy of 3.8 eV.

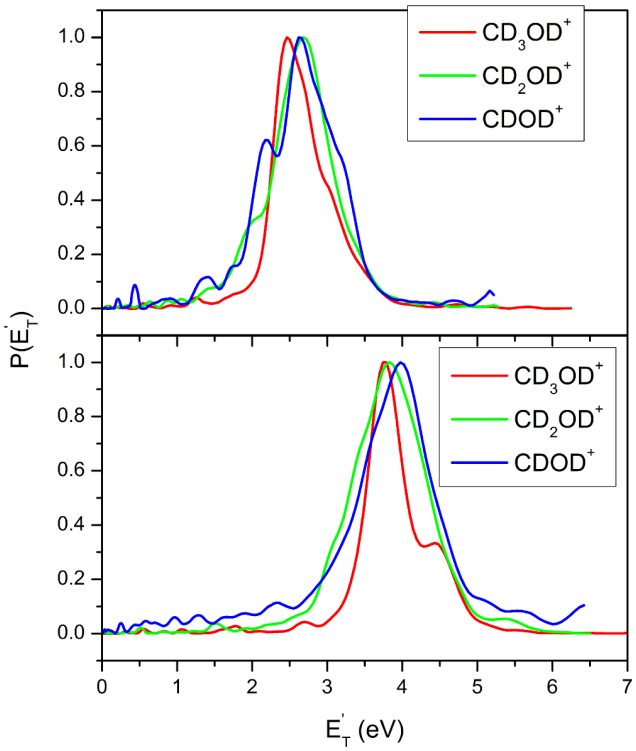

FIG. 3. Center of mass kinetic energy distributions for CD_3OD^+, CD_2OD^+, and $CDOD^+$ formation from $N^+ + CD_3OD$ at collision energies indicated. The top panel shows product formation at $E_{col} = 2.6$ eV, and the bottom panel of images corresponds to the formation of those same products at a collision energy of 3.8 eV. Horizontal axis is E_T', the relative translational energy of the products.

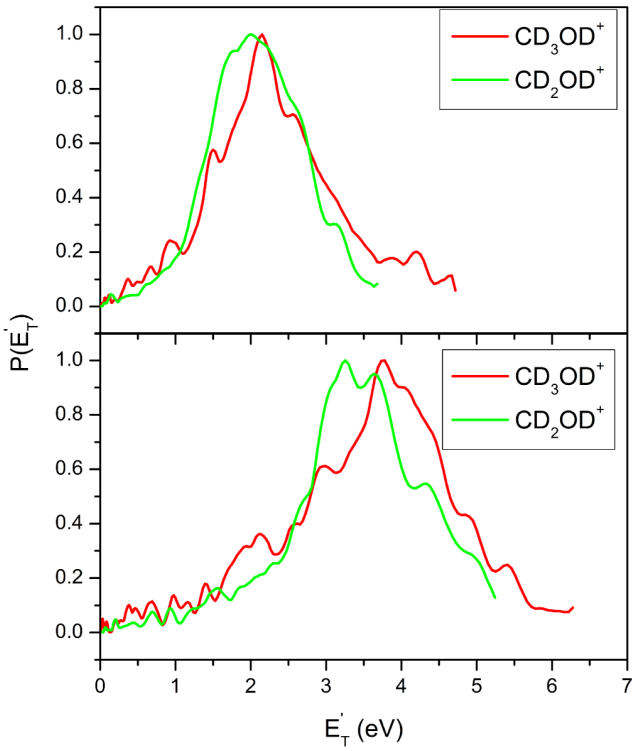

FIG. 4. Center of mass kinetic energy distributions for CD_3OD^+ and CD_2OD^+ formation from $O^+ + CD_3OD$ at collision energies indicated. The top panel shows product formation at $E_{col} = 2.0$ eV, and the bottom panel of images corresponds to the formation of those same products at a collision energy of 3.8 eV. Horizontal axis is E_T', the relative translational energy of the products.

tion yields a unique relationship between the speed of a single product and the relative velocity of the pair of separating products. The kinetic energy distributions for parent ion formation by charge transfer shown in Figures 3 and 4 are consistent with energy resonance, in which the most probable initial and final kinetic energies of the reactants and products are the same, although the distributions are significantly broader than the initial reactant distributions.

When the primary ion formed by charge transfer undergoes dissociation, however, the kinematics of the three-body dissociative process are formally indeterminate. As others[35–37] have shown, and as we have applied in the $N_2^+ + CH_4$ system,[38] when the kinetic energy release in the dissociation process is small, the assumption that all dissociation events behave as quasi-two-body processes is justifiable. That is, fragments such as $CD_2OD^+ + D$ are treated as a single particle with mass equal to the sum of the fragment masses. By setting the center of mass velocity vector **u** for the detected product equal to the CD_3OD^+ velocity determined by momentum matching to the accompanying N or O product, i.e., $|\mathbf{u}| = u_{CDOD^+} \approx u_{CD_2OD^+} \approx u_{CD_3OD^+}$, the final relative translational energy of the products is computed from the center of mass speed of the detected fragment through the relationship

$$E'_T = \frac{1}{2}\frac{m_{CD_3OD}}{m_{N/O}}Mu^2, \tag{7}$$

where M is the total mass of the collision system and u is the center of mass speed of the detected fragment ion. These assumptions have been made in constructing the fragment kinetic energy distributions of Figures 3 and 4. The congruence of the images and kinetic energy distributions for parent CD_3OD^+ and daughter CD_2OD^+ and $CDOD^+$ ions provides evidence supporting dissociative charge transfer as the dominant route for the formation of the daughter ions. Appreciable broadening of the daughter images relative to the parents would provide evidence against the foregoing assumptions, but we do not see any significant broadening.

By energy conservation, measurements of the kinetic energy distributions of the reaction products provide information on the internal energy distributions of parent CD_3OD^+ ions according to Eq. (8),

$$P(E'_{\text{int}}) = P(E_{total} - E'_T). \tag{8}$$

In this expression, E_{total} is the total energy available to the reagents, and is the sum of the incident kinetic energy, the reaction exoergicity, and the internal energies of reactants. The last contribution to E_{total} is essentially zero since the N^+ ions are formed in their ground electronic states, and the supersonic expansion cools the rotational energy of methanol isotopomers. Consistent with the energy resonant character of the initial charge transfer process, the most probable internal energies of the parent methanol ions are thus equal to the reaction exoercities: 356 kJ mol^{-1} (3.7 eV) and 268 kJ mol^{-1} (2.8 eV) for N^+ and O^+ reactants, respectively. In Sec. III B, we will present the explicit parent ion internal energy distributions and compare them with the positions of the excited electronic states of the methanol cation and the thresholds for forming fragment ions to help understand fragmentation pathways and product branching ratios.

An independent assessment of the internal energy distributions of methanol cations and their isotopomers can be obtained from the photoelectron spectra of CH_3OH, CH_3OD, and CD_3OD, whose features are governed largely by energy resonance and favorable Franck-Condon factors. Ionization of methanol occurs through the removal of one of the lone pair electrons on oxygen occupying a 2a″ orbital perpendicular to the C–O bond. The first band in the photoelectron spectrum of methanol, reported by MacNeil and Dixon,[39] is quite complex, exhibiting many overlapping features. The major contributors to activity in this band are the ν_5 CH_3 symmetric bending mode at 1456 cm^{-1} and the ν_7 CH_3 rocking mode at 1060 cm^{-1}. Activity in these methyl-based vibrations has been interpreted as evidence for a significant delocalization of electron density from the 2a″ orbital onto the carbon atom.

Although the kinetic energy distributions we observe do not show any structure associated with the vibrational bands that are expressed in the photoionization of methanol, in large part because the range of impact parameters involved in collisional ionization leads to significant rotational broadening of the kinetic energy distribution, it is worthwhile to compare the widths of the distributions prepared collisionally or by photon absorption. The most obvious differences in the distributions are the widths: the first band of the photoelectron spectrum is only 0.5 eV in width, but the kinetic energy distributions of the charge transfer products are somewhat broader. The product distributions from N^+ charge transfer are ~0.6 to 0.7 eV in width at both collision energies. The kinetic energy distributions for the products of dissociative ionization fall on top of the parent distributions, but exhibit slight broadening, some of which quite likely comes from the kinematic assumption that dissociative charge transfer is a quasi-two-body process.

Although one might expect that charge transfer collisions of O^+ with CD_3OD would exhibit kinetic energy distributions very similar to those for the N^+ collision partner, the distributions are markedly broader, ~1.5 to 1.7 eV in width. The data show more low velocity products in the case of collisions with O^+, further from the energy resonance condition, suggesting that charge transfer occurs in smaller impact interactions. The orientation dependence of the long range potential for approach of O^+ with its spherically symmetric electron density distribution, to methanol, will be significantly different from that of N^+, with its p-type symmetry in which the orientation of the occupied p orbital may lie perpendicular (Π-type) or parallel (Σ-type) to the relative velocity vector. These differences in the long range interaction potentials provide access to significantly different regions of the potential surface, with different Franck-Condon factors that control the widths of the internal energy distributions of the nascent parent ions.

B. Fragment ion formation

Experimental data to assess the loss of distinct hydrogen or deuterium atoms bound to carbon or oxygen were obtained by comparing the product intensities from CD_3OD and the partially deuterated methanol isotopomer CH_3OD. The product ion focusing conditions for velocity mapping are very different from the Wiley-McLaren conditions[40] that support optimal mass resolution, limiting our ability to resolve single

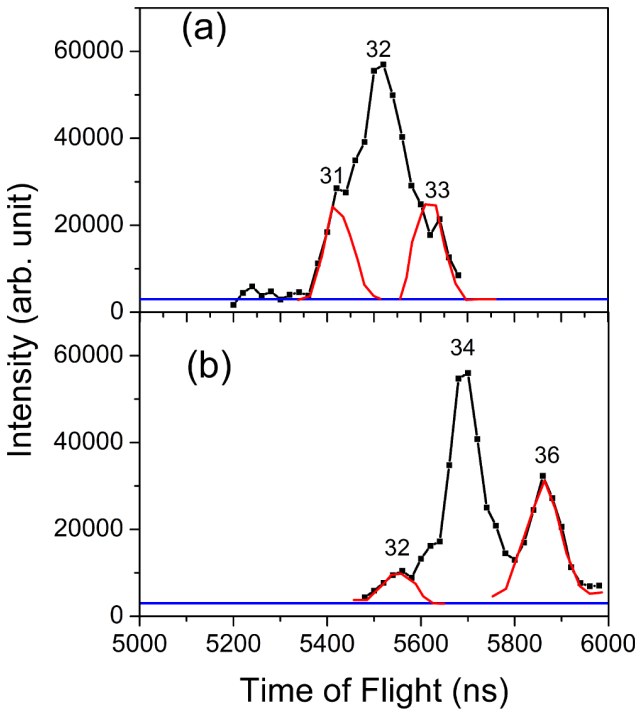

FIG. 5. Mass spectra of product ions in (a) N^+ + CH_3OD and (b) N^+ + CD_3OD collisions, obtained at collision energies of 2 eV, under velocity mapping conditions by signal-averaging product counts as functions of delay time from the detection extraction pulse. The red curves in (a) represent a fit to the 31 and 33 mass distributions. The red curves in (b) represent a fit to the 32 and 36 mass distributions.

mass number differences. However, comparing mass spectra with CH_3OD or CD_3OD reactants allows us to make clear product mass assignments. The upper panel of Figure 5 shows a typical mass spectrum for the products of $N^+ + CH_3OD$ collisions at a collision energy of 2 eV, showing a strong signal at m/e = 32 and weaker signals at m/e = 31 and 33, the latter incompletely resolved from the stronger 32 signal. The lower panel of Figure 5, for the $N^+ + CD_3OD$ system at 2 eV, exhibits similar behavior, with a strong signal at m/e = 34, corresponding to D atom loss, and weaker signals at m/e = 32 and m/e = 36 mass units. The experimental data for fragmentation of CH_3OD^+ show that all decay occurs through loss of hydrogen atoms, all of which are bound to the carbon atom. The data for fragmentation of CD_3OD^+ are consistent with the CH_3OD^+ data, and improved mass resolution afforded by deuterium substitution allows product intensity ratios to be determined.

It is well-known from the literature of mass spectrometry[41] that dissociative ionization of methanol and its isotopomers resulting in loss of a single hydrogen atom preferentially cleaves the C–H bond instead of the O–H bond. The mass spectrum of CH_3OD also shows that the $CHOD^+$ fragment is preferred over CH_2O^+ by nearly an order of magnitude. Therefore, the identities of the products of dissociative charge transfer reported here are compatible with those of dissociative ionization. In light of *ab initio* calculations[42,43] showing that the formaldehyde cation isomer is more stable than the hydroxymethylene cation, these results suggest that the fragmentation patterns are governed by kinetic rather than thermodynamic control.

The experimental data show that for N^++CD_3OD, approximately 40% of the product ion intensity can be assigned to the charge transfer parent CD_3OD^+, about 50% to loss of a single D atom, and 10% of the products correspond to loss of two deuterium atoms. At higher collision energy, charge transfer increases to 60%, D loss decreases to 30%, and the loss of two D atoms is responsible for ~10% of the product yield. The less exoergic O^+ + CD_3OD system forms two products: approximately 25% of the products correspond to CD_3OD^+ formed by charge transfer, with the majority of products assigned to CD_2OD^+ at low collision energy. At higher collision energy, charge transfer increases to 45% and loss of a single D atom drops to 55% of the total yield. The uncertainties in these product fractions are approximately 10%. Although our experiments are performed in an energy range where we should be able to detect CD_3^+ products from C–O bond cleavage, background signals from the ion beams of mass 14 or 16 interfered with the mass 18 CD_3^+ product, preventing us from observing this product.

The product branching ratios can be understood by considering energy deposition in the parent ions formed by charge

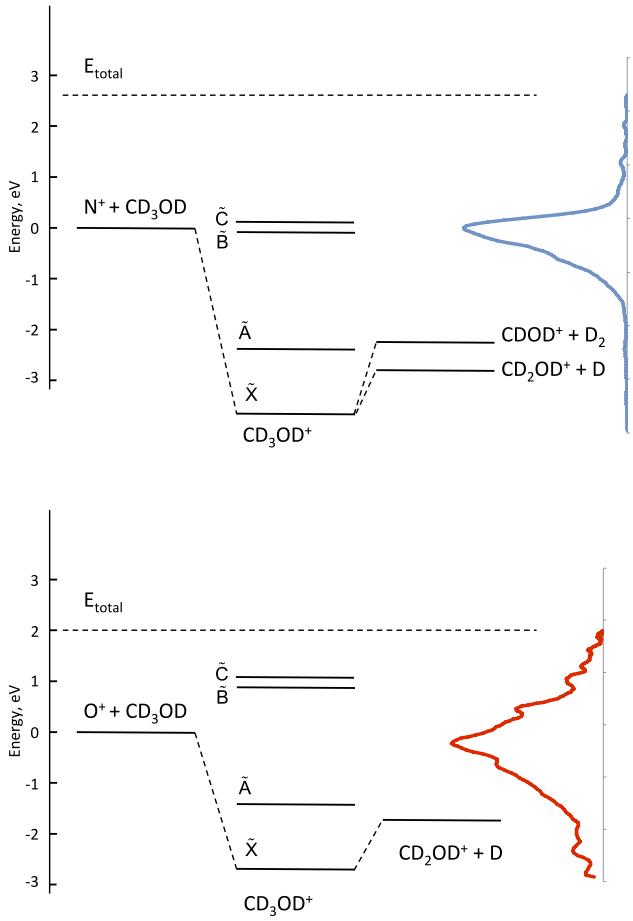

FIG. 6. Upper panel: reaction energy diagram for N^+ + CD_3OD, showing the internal energy distribution for CD_3OD^+ (blue curve) peaking at the energy resonance condition. Locations of the $\tilde{A}$, $\tilde{B}$, and $\tilde{C}$ excited states of the methanol cation are indicated, showing that the $\tilde{B}$ and $\tilde{C}$ states are preferentially excited. Lower panel: reaction energy diagram for O^+ + CD_3OD, showing the internal energy distribution for CD_3OD^+ (red curve) peaking at the energy resonance condition. The diagram shows that vibrationally excited levels of the $\tilde{A}$ state are excited preferentially. In both panels, the horizontal dashed lines define the incident kinetic energies.

transfer. In Figure 6, we show a schematic plot of the relative energies of reactants and products in the $N^+/O^+ + CD_3OD$ systems superimposed on the internal energy distributions of the products computed from Eq. (8). As we have noted earlier, resonant charge transfer constrains the internal energy distributions of the parent cations to be centered about the exoergicities of the charge transfer reactions, or up to 4 eV in the present experiments. Figure 6 also shows the positions of the energies of the excited $\tilde{A}$, $\tilde{B}$, and $\tilde{C}$ electronic states of methanol, determined from photoelectron-photoion coincidence (PEPICO) measurements, threshold photoelectron spectra (TPES), breakdown diagrams, and *ab initio* calculations reported by Borkar *et al.*[44]

In the top panel of Figure 6, the internal energy distribution for the CD_3OD^+ products shows clearly that the products of charge transfer are largely formed in the energy region where the $\tilde{B}$ and $\tilde{C}$ excited electronic states are accessible. Similarly, the lower panel of Figure 6 shows the same information for the $O^+ + CD_3OD$ reaction at the lower collision energy with two important differences: first, because of the lower exoergicity of the charge transfer process, the peak in the internal energy distribution of the parent ions falls well below the $\tilde{B}$ and $\tilde{C}$ state thresholds, but lies in the energy regime where vibrationally excited parent ions are formed in the $\tilde{A}$-state. Second, the internal energy distribution is significantly broader than for the N^+ system.

The PEPICO experiments show clearly that once the internal energies of the parent cations are above the C–H bond cleavage threshold at ~11.65 eV in CD_3OD, 0.8 eV above the ionization energy of methanol, the parent ion intensity is fully depleted over a very narrow range of internal energies approximately 0.2 eV in width, but the formation of CH_2OH^+ (CD_2OD^+ in our case) continues to occur several eV above threshold and is the predominant fragment at all parent ion internal energies up to 4 eV. The yield of CH_2OH^+ begins to decrease as parent ions dissociate via loss of two H-atoms to form $CHOH^+$, the yield of the latter increasing with increasing energy. As the parent internal energies reach the thresholds for the $\tilde{B}$ and $\tilde{C}$ electronic states, the C–O bond cleavage channel to form $CH_3^+ + OH$ opens, and the CH_2OH^+ yield drops further, reaching a value of 50% at 4 eV.

The internal energy distributions reflect those of stable rather than nascent products. The fact that the distributions preserve the energy resonant motif characteristic of many charge transfer reactions[45] leads us to believe that the partitioning of energy in stable methanol cation products is a good starting point for attempting to understand fragmentation in $N^+/O^+ + CD_3OD$ charge transfer.

The *ab initio* calculations reported by Borkar *et al.*[44] show that fragmentation of CD_3OD^+ by C–D bond cleavage occurs only in the $\tilde{X}$ state of the parent cation. Parent ions formed in the excited $\tilde{A}$ state may fragment by internal conversion to excited vibrational levels of the ground state. However, parent ions formed in the excited $\tilde{B}$ and $\tilde{C}$ states may undergo direct dissociation to $CH_3^+ + OH$ by C–O bond cleavage, or may undergo internal conversion to high vibrational levels of the $\tilde{A}$ or $\tilde{X}$ states, ultimately yielding CH_2OH^+ products. The breakdown diagram suggests that parent ions with excitation levels equivalent to the energies of $\tilde{B}$ or $\tilde{C}$ states fragment directly to CH_3^+ roughly half the time, or relax in the electronic manifold and fragment CH_2OH^+ or $CHOH^+$ the remainder of the time.

This information leads us to conclude that the pathway for dissociation by C–H(D) bond cleavage in nascent parent ions formed in excited electronic states occurs via internal conversion and vibrational relaxation to the parent ion ground state from those excited states. This picture is consistent with Quasi Equilibrium Theory (QET) of mass spectrometry[46] and suggests that parent ion fragmentation takes place statistically. In small molecules such as CH_3OH^+ (CD_3OD^+), the densities of vibrational states in the electronic states may be sufficiently sparse to prevent the statistical limit from being reached. More specifically, the efficiency of the relaxation processes will depend on Franck-Condon factors and coupling strengths at specific regions of the potential surfaces where internal conversion takes place.[47,48]

It is particularly interesting to examine the differences in the internal energy distributions of CD_3OD^+ products formed in collisions of the neutral precursor with N^+ and O^+. Figure 6 suggests that the larger exoergicity of the N^+ reaction populates the $\tilde{B}$ and $\tilde{C}$ states at low levels of internal excitation. In contrast, the smaller exoergicity of the O^+ reaction results in the formation of products in high vibrational levels of the $\tilde{A}$ state. Franck-Condon overlaps for vibrationally excited levels of the $\tilde{A}$ state with excited levels of the $\tilde{X}$ state may be significantly more favorable in this case, providing a mechanism for forming the ground state parent cation in a highly excited configuration that produces a higher C–D bond cleavage yield. The smaller yield of the CD_2OD^+ fragment for the more exoergic reaction with N^+ reflects the fact that an additional product, CD_3^+, is formed.

Charge transfer is generally controlled by long range potential surface crossings whose locations are sensitive to the details of the approaching reactants. The approaching O^+ ion is spherically symmetric and is expected to have very different interactions with methanol compared to N^+ with its p-type symmetry. It is well-known[49] that p-state species may interact with collision partners through Σ-type interactions, in which the electron density of the approaching ion lies along the relative velocity vector, or via Π-type interactions in which the electron density is oriented perpendicular to the relative velocity. Such stereochemical effects can lead to significant differences in the locations of surface crossings and therefore the specific energy content of the nascent methanol cation. These issues will require additional detailed theoretical efforts for a complete understanding.

Although the congruence of the velocity map images, and therefore the kinetic energy and angular distributions, for non-dissociative and dissociative charge transfer producing CH_3OD^+ and CH_2OD^+ and isotopomers, suggests that hydrogen atom loss can be explained by charge transfer, we must also examine the putative role of hydride transfer. Hydride transfer requires a vacant atomic orbital to accommodate an electron pair, and the process generally takes place with significant kinetic energy release. An early crossed beam study from our lab on the $C^+ + CH_3OH$ system[17] showed that charge transfer was energy resonant, like the N^+ and O^+ systems reported here, but that hydride transfer to form CH_2OH^+ led

to significant disposal of the reaction exoergicity into product translation. In the collision energy range between 1 and 3 eV, the product kinetic energy release for hydride transfer was 0.6 to 0.8 eV larger than the energy resonant values for charge transfer. Facile hydride transfer from CH_3OH occurs for C^+ reactants, in which two 2p-orbitals are vacant, but does not appear to occur for N^+ or O^+ reactants, although N^+ has a single vacant orbital. The reason that hydride transfer is suppressed for this ion is unclear, and requires a higher level of theoretical understanding.

Hydride transfer and dissociative charge transfer appear to have significantly different dynamical signatures in the $C^+ + CH_3OH$ system. It is very reasonable to expect that if both processes were operative in the N^+ and O^+ systems, the data would allow hydride transfer and dissociative charge transfer to be discriminated both through energy disposal and by their differing collision energy dependences. Therefore, the observation that CH_2OD^+/CD_2OD^+ products formed with N^+ and O^+ reactants have images and product energy and angular distributions that are congruent with the charge transfer products provides strong evidence that dissociative charge transfer rather than hydride transfer is responsible for the formation of these products.

C. Is NO^+ formed?

In the $N^+ + CH_3OH$ system, the $CHOH^+$ product expected from loss of two hydrogen atoms from the CH_3OH^+ parent ion is isobaric with NO^+. NO^+ could conceivably be formed by attack of N^+ on the oxygen atom, followed by hydrogen atom migration to the carbon atom and C–O bond cleavage. The lower ionization potential of NO (9.26 eV) compared to CH_4 (12.61 eV) is consistent, via Stevenson's rule[50] with the charge residing on NO^+. The results of Smith, Adams, and Miller[6] for the formation of reaction products with m/e = 30 showed a peculiar biexponential behavior that the authors speculated could be associated with NO^+ production, and reported a branching fraction of 0.10 for this product at thermal energy.

By employing CD_3OD, we can distinguish between the reaction product CD_2O^+ formed by loss of two D atoms (m/e = 32) and the NO^+ product at m/e = 30. Experiment demonstrates that m/e = 30 product formation is below the detection limit. This observation does not rule out the possibility that NO^+ is formed at thermal energies, where the lifetime of the putative intermediate leading to NO^+ should be much longer, but it does mitigate strongly against formation of that product.

IV. CONCLUSIONS

The reactive systems $N^+ + CD_3OD$ and $O^+ + CD_3OD$ exhibit several dynamical signatures that add to the preliminary understanding that rate studies have established. Velocity map imaging has established that the reactions the species undergo are initiated by resonant charge transfer. The kinetic energy distributions associated with charge transfer are significantly broader than the Franck-Condon profiles for photoionization. Reaction energetics show that nascent parent ions are formed in excited electronic states that undergo internal conversion and vibrational relaxation prior to dissociation to form CD_2OD^+ products. The experimental data also show that loss of a deuterium atom from the parent ion takes place via dissociative charge transfer rather than hydride abstraction. Isotope labeling studies show that this loss of deuterium occurs from the carbon atom, consistent with the electron impact mass spectrum of methanol. Finally, isotopic substitution allows us to eliminate the possibility that a complex rearrangement process involving attack of N^+ on the oxygen atom in methanol is a pathway to NO^+ production.

ACKNOWLEDGMENTS

The authors acknowledge support for this work under National Science Foundation Grant Nos. CHE-1012303 and CHE-1265406.

[1]E. E. Ferguson, Rev. Geophys. **12**, 703, doi:10.1029/RG012i004p00703 (1974).
[2]A. Chen, R. Johnsen, and M. A. Biondi, J. Chem. Phys. **69**, 2688 (1978).
[3]A. V. Pavlov, Surv. Geophys. **33**, 1133 (2012).
[4]The online database KIDA (V. Wakelam *et al.*, 2012, http://kida.obs.u-bordeaux1.fr) is a comprehensive compendium of important reactions and rates.
[5]D. J. Levandier, Y. H. Chiu, R. A. Dressler, L. P. Sun, and G. C. Schatz, J. Phys. Chem. A **108**, 9794 (2004).
[6]D. Smith, N. G. Adams, and T. M. Miller, J. Chem. Phys. **69**, 308 (1978).
[7]N. G. Adams, D. Smith, and J. F. Paulson, J. Chem. Phys. **72**, 288 (1980).
[8]W. A. Chupka and M. E. Russell, J. Chem. Phys. **48**, 1527 (1968).
[9]L. Pei and J. M. Farrar, Int. J. Mass Spectrom. **377**, 93 (2015).
[10]W. T. Huntress and V. G. Anicich, Geophys. Res. Lett. **3**, 317, doi:10.1029/GL003i006p00317 (1976).
[11]V. G. Anicich, W. T. Huntress, and J. H. Futrell, Chem. Phys. Lett. **47**, 488 (1977).
[12]M. Tichy, A. B. Rakshit, D. G. Lister, N. D. Twiddy, N. G. Adams, and D. Smith, Int. J. Mass Spectrom. Ion Phys. **29**, 231 (1979).
[13]S. Dheandhanoo, R. Johnsen, and M. A. Biondi, Planet. Space Sci. **32**, 1301 (1984).
[14]J. B. Marquette, B. R. Rowe, G. Dupeyrat, and E. Roueff, Astron. Astrophys. **147**, 115 (1985).
[15]B. R. Rowe, J. B. Marquette, G. Dupeyrat, and E. E. Ferguson, Chem. Phys. Lett. **113**, 403 (1985).
[16]J. Zabka, M. Farnik, Z. Dolejsek, J. Polach, and Z. Herman, J. Phys. Chem. **99**, 15595 (1995).
[17]R. A. Curtis and J. M. Farrar, Chem. Phys. Lett. **123**, 471 (1986).
[18]R. A. Curtis and J. M. Farrar, J. Chem. Phys. **90**, 862 (1989).
[19]L. Liu, E. S. Richards, and J. M. Farrar, J. Chem. Phys. **127**, 244315 (2007).
[20]T. Schindler, C. Berg, G. Niedner-Schatteburg, V. E. Bondybey, C. Lugez, A. Schriver, and L. Schriver, J. Phys. Chem. **98**, 4316 (1994).
[21]A. Eppink and D. H. Parker, Rev. Sci. Instrum. **68**, 3477 (1997).
[22]*Thermodynamic Parameters Taken From NIST Chemistry WebBook, NIST Standard Database Number 69*, edited by W. G. Mallard and P. J. Linstrom (National Institute of Standards and Technology, Gaithersburg, MD, 2000), http://webbook.nist.gov/chemistry/.
[23]L. Pei and J. M. Farrar, J. Chem. Phys. **136**, 204305 (2012).
[24]E. L. Reichert, S. S. Yi, and J. C. Weisshaar, Int. J. Mass Spectrom. **196**, 55 (2000).
[25]E. L. Reichert, G. Thurau, and J. C. Weisshaar, J. Chem. Phys. **117**, 653 (2002).
[26]E. L. Reichert and J. C. Weisshaar, J. Phys. Chem. A **106**, 5563 (2002).
[27]J. Mikosch, U. Fruhling, S. Trippel, D. Schwalm, M. Weidemuller, and R. Wester, Phys. Chem. Chem. Phys. **8**, 2990 (2006).
[28]J. Mikosch, S. Trippel, C. Eichhorn, R. Otto, U. Lourderaj, J. X. Zhang, W. L. Hase, M. Weidemuller, and R. Wester, Science **319**, 183 (2008).
[29]J. X. Zhang, J. Mikosch, S. Trippel, R. Otto, M. Weidemuller, R. Wester, and W. L. Hase, J. Phys. Chem. Lett. **1**, 2747 (2010).
[30]H. Udseth, C. F. Giese, and W. R. Gentry, Phys. Rev. A **8**, 2483 (1973).
[31]R. D. Smith and J. H. Futrell, J. Chem. Phys. **65**, 2574 (1976).
[32]D. Smith, P. Spanel, and C. A. Mayhew, Int. J. Mass Spectrom. Ion Processes **117**, 457 (1992).
[33]D. Townsend, M. P. Minitti, and A. G. Suits, Rev. Sci. Instrum. **74**, 2530 (2003).

[34]V. Dribinski, A. Ossadtchi, V. A. Mandelshtam, and H. Reisler, Rev. Sci. Instrum. **73**, 2634 (2002).
[35]Z. Herman, J. H. Futrell, and B. Friedrich, Int. J. Mass Spectrom. Ion Processes **58**, 181 (1984).
[36]A. K. Shukla, K. G. Qian, S. L. Howard, S. G. Anderson, K. W. Sohlberg, and J. H. Futrell, Int. J. Mass Spectrom. Ion Processes **92**, 147 (1989).
[37]A. K. Shukla, K. Qian, S. Anderson, and J. H. Futrell, J. Am. Soc. Mass Spectrom. **1**, 6 (1990).
[38]L. Pei and J. M. Farrar, J. Chem. Phys. **138**, 124304 (2013).
[39]K. A. G. Macneil and R. N. Dixon, J. Electron Spectrosc. Relat. Phenom. **11**, 315 (1977).
[40]W. C. Wiley and I. H. McLaren, Rev. Sci. Instrum. **26**, 1150 (1955).
[41]J. H. Beynon, A. E. Fontaine, and G. R. Lester, Int. J. Mass Spectrom. Ion Phys. **1**, 1 (1968).
[42]M. J. Frisch, K. Raghavachari, J. A. Pople, W. J. Bouma, and L. Radom, Chem. Phys. **75**, 323 (1983).
[43]Y. Osamura, J. D. Goddard, H. F. Schaefer, and K. S. Kim, J. Chem. Phys. **74**, 617 (1981).
[44]S. Borkar, B. Sztaray, and A. Bodi, Phys. Chem. Chem. Phys. **13**, 13009 (2011).
[45]J. B. Laudenslager, W. T. Huntress, and M. T. Bowers, J. Chem. Phys. **61**, 4600 (1974).
[46]H. M. Rosenstock, M. B. Wallenstein, A. H. Wahrhaftig, and H. Eyring, Proc. Natl. Acad. Sci. U. S. A. **38**, 667 (1952).
[47]G. W. Robinson and R. P. Frosch, J. Chem. Phys. **37**, 1962 (1962).
[48]G. W. Robinson and R. P. Frosch, J. Chem. Phys. **38**, 1187 (1963).
[49]V. Aquilanti, M. Bartolomei, F. Pirani, D. Cappelletti, F. Vecchiocattivi, Y. Shimizu, and T. Kasai, Phys. Chem. Chem. Phys. **7**, 291 (2005).
[50]D. P. Stevenson, Discuss. Faraday Soc. **10**, 35 (1951).